

Accepted for publication by Physical Review D.

Revised on March 10, 2000.

Properties of Regge Trajectories

Alfred Tang and John W. Norbury

Physics Department, University of Wisconsin - Milwaukee,

P. O. Box 413, Milwaukee, WI 53201.

Emails: atang@uwm.edu, norbury@uwm.edu

Abstract

Early Chew-Frautschi plots show that meson and baryon Regge trajectories are approximately linear and non-intersecting. In this paper, we reconstruct all Regge trajectories from the most recent data. Our plots show that meson trajectories are non-linear and intersecting. We also show that all current meson Regge trajectories models are ruled out by data.

PACS numbers: 11.55.J, 12.40.Nn, 14.20.-c, 14.40.-n.

1 Introduction

The topic of Regge trajectories was an active area of research in the 1960's. But there is a resurgence of interest in Regge trajectories because of the quantity of new data that need analysis and the new quark models need more complete experimental fits for testing. Despite these recent interests, some authors [1, 2] are still using old data to construct Chew-Frautschi plots. In this paper, we reconstruct all Regge trajectories with the most recent data and elucidate the principles of their construction. At the end, we explain why all current meson Regge trajectories models are ruled out by data.

1.1 Theoretical Developments

This paper is concerned with the properties of Regge trajectories which are graphs of the total quantum number J versus mass squared M^2 over a set of particles of fixed principal quantum number N , isospin I , dimensionality of the symmetry group D , spin-parity and flavor. Variations in J and L ($J = L + S$) are equivalent when S is fixed.

Scattering processes are usually analyzed by the method of partial-waves [3, 4]. The wavefunction in the far zone has the form

$$\psi(\mathbf{r}) \simeq e^{i\mathbf{k}\cdot\mathbf{r}} + f(k, \cos \theta) \frac{e^{i\mathbf{k}\cdot\mathbf{r}}}{r}, \quad (1)$$

where θ is the angle between the wave vector \mathbf{k} and the position vector \mathbf{r} . In the case of bound states, the plane wave term is absent. The form factor f is written as a sum of partial-waves as

$$f(k^2, \cos \theta) = \sum_{l=0}^{\infty} (2l+1) a_l(k^2) P_l(\cos \theta), \quad (2)$$

$$a_l(k^2) = \frac{1}{2} \int_{-1}^1 f(k^2, \cos \theta) P_l(\cos \theta) d \cos \theta, \quad (3)$$

where l is the orbital angular momentum quantum number and P_l is the Legendre polynomial of order l . In 1959, Regge [5, 6] generalized the solution of f by complexifying angular momenta. He interpreted the simple poles of $a_l(k^2)$ on the complex l -plane to be either resonances or bound states.

Chew and Frautschi [7] applied the Regge poles theory to investigate the analyticity of $a_l(k^2)$ in the case of strong interactions. They postulated that all strongly interacting particles are self-generating (the bootstrap hypothesis) and that they must lie on Regge trajectories (Chew-Frautschi conjecture) [8].

At first, linearity was just a convenient guide in constructing the Chew-Frautschi plots because data were scarce and there were few *a priori* rules to direct the mesons and baryons into the same trajectories [9]. Once linearity was found to be a good working hypothesis, justification was given through certain assumptions in the Regge poles theory as follows: For $\text{Re } l \geq -1/2$, the partial-wave components of the scattering amplitude f have only simple poles and are functions of k^2 ,

$$a_l(k^2) \simeq \frac{\beta(k^2)}{l - \alpha(k^2)}, \quad (4)$$

where β is the residue (Regge residue) and α the position (Regge trajectory) of the simple poles. We can use Watson transformation to rewrite Eq. [2] as the Sommerfeld-Watson formula [10] to include the poles.

A Regge trajectory $J = \alpha(k^2)$ is also sometimes expressed as $J = \alpha(E)$, or more commonly in terms of the Mandelstam variable t as $J = \alpha(t)$. t is the center-of-mass energy of the quark-antiquark pair defined as $t \equiv (p_q + p_{\bar{q}})^2$. It is used instead of s or u because Regge poles generally arise in this channel. For the purpose of plotting, we use $J = \alpha(M^2)$. $\alpha(t)$ represents a set of leading Regge poles on the complex l -plane and is called the Reggeon. The condition $\alpha(t) < 0$ does not correspond to any physical particles because J cannot be negative [11].

Many authors [9, 13] are careful to disclaim linearity as being only approximate. For others, linearity is simply stated [14, 15]. By and large, it is believed that Regge trajectories for relativistic scattering are straight lines over a considerable range of energy without any sign of deviation [16, 17, 18]. Attempts have been made to validate this belief on computational grounds. Kahana, Maung and Norbury [19] calculated the numerical solutions of the relativistic Thompson equation which yield linear, non-intersecting and parallel Regge trajectories. Their calculation did not include the effects of spin which can be a factor in predicting the shape of the Regge trajectories. But earlier in 1985, Godfrey and Isgur [20] solved a relativized Schrödinger equation which did include the spin-spin and spin-orbit interactions. Their calculation concurred with the results of linear Regge trajectories obtained from spinless particles. These two works together seem to suggest that the effect of spin on the shape of the Regge trajectories is negligible. On the other hand, if the coupling constants are not negligible, one expects the spin-orbit contributions to be significant for high J values. Salvo [1] *et al.* published solutions for non-linear Regge trajectories by including spin dependent terms in a 3-dimension reduction of the Bethe-Salpeter equation. Salvo's conclusion differs from those of Kahana and Godfrey concerning the effect of spin on Regge trajectories.

The linearity of Regge trajectories has been the object of investigation once again recently. On the theoretical front, Tang [21] used perturbative QCD to show that Regge trajectories are non-linear by studying high-energy elastic scattering with mesonic exchange in the case of both fixed and running coupling constants. On the experimental side, Brandt [22] *et al.* affirmed the existence of non-linear Pomeron trajectories from the data analysis of the recent UA8 and ISR experiments at CERN. They published a

parameterization of Pomeron trajectories containing a quadratic term,

$$\alpha(t) = 1.10 + 0.25t + \alpha''t^2. \quad (5)$$

where α'' is a constant. Recently, Burakovsky [23, 24] presented a phenomenological string model for logarithmic and square root Regge trajectories.

In this paper, we check the claims of non-linear Regge trajectories by plotting the most recent experimental data published in the 1998 Review of Particle Physics (RPP) [25]. Our plots confirm the existence of non-linear trajectories. Early Chew-Frautschi plots also show that Regge trajectories fan out. We refer to this non-intersecting property as “divergence.” We also show that many trajectories intersect. Kahana et al. numerically constructed a set of hypothetical Regge trajectories by using a fully relativistic Thompson equation. They discovered that there are differences in the properties of the trajectories obtained by NRSE versus those by the Thompson equation. We summarize the conclusions of Kahana et al. in Table 1 to illustrate these differences.

Table 1: Comparisons of the predictions made by NRSE and the relativistic Thompson equation according to Kahana et al. [19]. “Yes” refers to a property predicted by the theory and “No” is the prediction of the opposite property.

	Non-relativistic Schrödinger Equation	Relativistic Thompson Equation
Linearity	No	Yes
Divergence	No	Yes
Parallelism	Yes	Yes

When trajectories of different principal quantum numbers N but all other quantum numbers fixed are plotted together, they appear parallel. We call this property “parallelism.”

1.2 Construction of Regge Trajectories

The starting point for constructing a meson Regge trajectory is the meson assignment table in RPP (Table 13.2 on p. 110 of Ref. [25]). We fix I and flavor by selecting particles

from a single column. From this column, we isolate different trajectories by fixing N and spin-parity when we select particles with consecutive values of J . For example, the 1^1S_0 , 1^1P_1 and 1^1D_2 states constitute an $N = 1$ singlet trajectory; 1^3P_0 and 1^3D_1 the $N = 1$ first triplet; 1^3P_1 and 1^3D_2 the $N = 1$ second triplet; 1^3S_1 , 1^3P_2 , 1^3D_3 , and 1^3F_4 the $N = 1$ third triplet; 2^3S_1 and 2^3P_2 the $N = 2$ third triplet and so on. We use the experimental error instead of the width to measure the accuracy of the mass of a meson. The width measures the imaginary part of the complex energy while the experimental error indicates the accuracy of the measurement of the mass at the resonance peak. In case the mass of both the neutral and charged mesons are reported, the mass is taken to be the average of the three. For example, the mass of $\pi(138)$ is taken to be the average mass of $\pi^0(135)$ and $\pi^\pm(140)$. Similarly the error of mass is also taken to be the average of the errors of the two corresponding masses. This scheme does not pose any serious ambiguity because the masses and the errors of the neutral and charged mesons are usually quite close (the difference in mass is usually $< 1\%$ and is $\sim 3.5\%$ in the worst case) and hence do not change our conclusions. The error of mass square, dM^2 , is calculated from the mass M and its error dM by the relation $dM^2 = 2MdM$. The end results are 13 trajectories containing 2 particles each, 4 containing 3 particles each and 4 containing 4 particles each. Single particle trajectories are omitted from the plots. None of the $N = 1$ second triplet trajectories are plotted because most of them are single particle trajectories except the one containing K_{1B} and $K_2(1820)$, where K_{1B} is a nearly equal (45°) mixture of $K_1(1270)$ and $K_1(1400)$. Since some of these trajectories contained unconfirmed mesons, not all of them are used in this paper.

The bold face entries in the assignment table refer to the mesons which are confirmed by experiments. The regular typeface entries correspond to those which are omitted from the summary table because of work in progress. For example, one of the regular typeface entries in the assignment table, $f_4(2220)$, is listed as $f_J(2220)$ in the summary table because J may assume a value of either 2 or 4 depending on the final confirmation by experiments. There are other similar undetermined quantities in the meson data. This paper takes the conservative approach by using only the bold face (confirmed) data contained in the RPP meson assignment table.

The baryon Regge trajectories are constructed from the RPP baryon assignment table (Table 13.4 on p. 112 of Ref. [25]). Baryons are categorized into 4 different confidence levels according to their likelihood of existence. Confidence level 1 is assigned to the baryons which are deemed the least likely to exist and level 4 the most likely to exist. The baryon assignment table contains only the level 3 and 4 particles. These are the

baryons we will analyze in this paper.

The baryon assignment table uses a set of slightly different quantum numbers, such as J^P , (D, L_N^P) and S . As before, J is the total angular momentum, P the parity, L the orbital angular momentum and S the spin. The new quantum number D is the dimensionality of the symmetry group and has the value of either 56 or 70. These numbers come from the dimensionalities of the irreducible representations of flavor-spin $SU(6)$, i.e. $\mathbf{6} \otimes \mathbf{6} \otimes \mathbf{6} = \mathbf{56}_S \oplus \mathbf{70}_M \oplus \mathbf{70}_M \oplus \mathbf{20}_A$ where the subscript S stands for “symmetric”, A for “asymmetric” and M for “mixed symmetry.” N is the “band” which gives the number of excitation quanta. The construction of a baryon Regge trajectory is similar to that of the meson in that all quantum numbers except J are fixed along a trajectory. In other words, D , S , flavor, strangeness and isospin are constant along a baryon Regge trajectory. Only L is allowed to vary. N changes with L in the same integer steps so that a change in N is the same as a change in L . Hence we can ignore the consideration of N .

Regge recurrences are separated by 2 units of J . In the case of mesons, we can plot two trajectories together in some cases because the cross channel forces between them vanish. It is known as the “exchange degeneracy” (EXD) [13] which arises out of the cross channel forces which split $a(l, k)$ into even (+) and odd (−) signatures as $a_{\pm}(l, k)$. The separation of the even and odd signatures correspond to the two different Regge trajectories. If the cross channel forces vanish (as in the case of mesons), the even and odd signatures coincide and the even and odd trajectories overlap. It means $\alpha_+ = \alpha_-$ and $\beta_+ = \beta_-$. These are called the EXD conditions. When the EXD conditions apply, the even and odd parity mesons can be plotted along the same trajectories. In the case of baryons, the cross channel forces persist. Therefore the even and odd parity baryons cannot be plotted together in the same trajectories. The EXD criteria enable us to pick out 3 trajectories of 3 baryons each and 2 trajectories of 2 baryons each from the baryon assignment table. These selections are achieved by isolating a column (e.g. the $N(939)$ – $N(2220)$ column) and picking all the particles with the same D , S and P (e.g. $N(939)$, $N(1680)$ and $N(2220)$). Once a trajectory is picked from the first column, corresponding entries of the following columns also constitute baryon Regge trajectories. The spectroscopic notation for baryons is $L_{2I,2J}$. The N and Λ trajectories are made up of the P_{11} , F_{15} , H_{19} states and the Δ trajectory is made up of the P_{33} , F_{37} , H_{311} states.

2 Linearity

Linearity means that all the particles of a Regge trajectory must lie on the straight line $M^2 = \alpha J + \beta$. In graphical analysis, non-linearity can be detected by simple inspection in only extreme cases. Linearity on the other hand is more difficult to judge. Therefore we devise a method called the “zone test” to facilitate this judgment.

2.1 Zone Test

We test linearity by the “zone test” on Regge trajectories with 3 or more particles. A test zone of an experimental Regge trajectory is defined to be the area bounded by the error bars of the first and the last particles and the straight lines joining them. Figs. 1–6 illustrate these test zones (regions enclosed by the dotted lines). A zone contains all the possible straight lines crossing the error bars of the first and the last particles. A Regge trajectory can be a straight line if the error bars of all other particles intersect the zone. In most cases, intersections are easily discernible by inspection. If ambiguity ever arises in borderline cases, an exact numerical version of the zone test is used.

Suppose we are given a sequence of N mesons and their values of mass square with errors, $\{M_i^2 \pm dM_i^2\}$. We calculate the equation of the straight line connecting $M_1^2 + dM_1^2$ and $M_N^2 + dM_N^2$ and then the equation of the line connecting $M_1^2 - dM_1^2$ and $M_N^2 - dM_N^2$. These two lines define the boundaries of the zone. For each J , we can calculate the bounds to be intersected by the error bar to qualify as a linear Regge trajectory. For a 3-particle trajectory in which the particles are labelled (1, 2, 3), the lower and upper bounds at $J = 2$ are calculated as

$$\begin{aligned} lb(3, 2) &= \frac{(M_1^2 - dM_1^2) + (M_3^2 - dM_3^2)}{2}, \\ ub(3, 2) &= \frac{(M_1^2 + dM_1^2) + (M_3^2 + dM_3^2)}{2}, \end{aligned} \quad (6)$$

where $lb(3, 2)$ stands for the lower bound and $ub(3, 2)$ the upper bound of particle 2 along a 3-particle trajectory. Similarly, we can calculate the bounds of particles 2 and 3 along a 4-particle trajectory as

$$\begin{aligned} lb(4, 2) &= \frac{2(M_1^2 - dM_1^2) + (M_4^2 - dM_4^2)}{3}, \\ ub(4, 2) &= \frac{2(M_1^2 + dM_1^2) + (M_4^2 + dM_4^2)}{3}. \end{aligned} \quad (7)$$

$$\begin{aligned}
lb(4, 3) &= \frac{(M_1^2 - dM_1^2) + 2(M_4^2 - dM_4^2)}{3}, \\
ub(4, 3) &= \frac{(M_1^2 + dM_1^2) + 2(M_4^2 + dM_4^2)}{3}.
\end{aligned} \tag{8}$$

We can generalize these results for particle i along an n -particle trajectory as

$$\begin{aligned}
lb(N, i) &= \frac{(N - i)(M_1^2 - dM_1^2) + (i - 1)(M_N^2 - dM_N^2)}{N - 1}, \\
ub(N, i) &= \frac{(N - i)(M_1^2 + dM_1^2) + (i - 1)(M_N^2 + dM_N^2)}{N - 1}.
\end{aligned} \tag{9}$$

This numerical method is useful for checking linearity when simple inspection is inconclusive.

2.2 Conclusions from Zone Test

All of the data points in all of the graphs in this paper are shown with error bars. If the error bars are invisible in the plots, it simply means that the error bars are smaller than the symbols of the associated data points. We use the zone test to check linearity by simple inspection in Figs. 1–6. At least one of the error bars of the intermediate particles fails to intersect the test zone in all of the figures except Fig. 3.

Figs. 1–2 illustrate a group of meson Regge trajectories of the $N = 1$, $S = 0$ singlet states and varying J corresponding to the 1^1S_0 , 1^1P_1 and 1^1D_2 states. Both trajectories fail the zone test and are non-linear. The π trajectory has a decreasing slope.

In Figs. 3–6, trajectories of the $N = 1$, $S = 1$ third triplet states with varying J corresponding to the 1^3S_1 , 1^3P_2 , 1^3D_3 , and 1^3F_4 states are plotted. Trajectories in Figs. 4 and 6 fail the zone test by simple inspection. In Fig. 3, the error bars of both $a_2(1320)$ and $\rho_3(1690)$ appear to intersect the zone at the lower boundary. In this case, the numerical version of the zone test is used. The error bars of both particles must intersect the bounds to support linearity. The bounds in the case of $a_2(1320)$ are $(lb, ub)(4, 2) = (1.73, 1.78) \text{ GeV}^2$ which intersect the error bar, $(1.7358, 1.7390) \text{ GeV}^2$. The bounds for $\rho_3(1690)$ are $(lb, ub)(4, 3) = (2.87, 2.96) \text{ GeV}^2$ which also intersect the error bar, $(2.843, 2.876) \text{ GeV}^2$. The numerical test supports the existence of a straight line intersecting all the error bars of the particles along this trajectory. The ω trajectory has an increasing slope while both the ϕ and K^* trajectories have decreasing slopes.

The zone test for baryon trajectories are illustrated in Figs. 7–9. The N and Δ trajectories in Figs. 7 and 9 clearly satisfy the zone test by simple inspection. The Λ

trajectory in Fig. 8 is shown to be non-linear by the numerical zone test. In summary, 6 of 8 trajectories with 3 or more particles each are shown to be non-linear. Polynomial fits of the trajectories are included in the figure captions for reference only.

3 Divergence

Divergence seems to be a property of the Regge trajectories in the early Chew-Frautschi plots and is also a prediction of the numerical calculations by Kahana et al [19]. Divergence is defined to be the conjunction of two properties: (1) non-intersection and (2) fanning out.

We check divergence by plotting families of meson Regge trajectories with the same isospin and spin-parity in Figs. 10–15. It is observed that non-linear trajectories of similar masses intertwine. In general, Regge trajectories are not evenly separated in a graph. Some trajectories can be obscured when many of them are plotted over a large mass range on the same graph. We adopt a numeration scheme which allows us to identify the obscured trajectories in separate plots. For example, the group denoted as 1–3 in Fig. 11 is magnified as trajectories 1–3 in Fig. 12. Divergence is clearly violated in Fig. 14 when trajectories intersect. Due to the large error bars, divergence in Fig. 12, the determination of the properties of these meson trajectories is inconclusive.

Although individual meson trajectories do not fan out, it can be seen in Figs. 10, 11, 13 and 15 that groups of them diverge on a global level. We also notice that these groups can be labelled according to mass difference. In general, the mass of the intersecting trajectories does not differ significantly. On the other hand, divergent trajectories have large mass difference. For example, in Fig. 10, the π , K and η trajectories have small mass difference and form a group of intersecting trajectories. The D and D_S trajectories also form a group with small mass difference. These two groups of trajectories diverge globally. In summary, trajectories of small mass difference do not diverge but those of large mass difference fan out in our plots. In the case of baryon Regge trajectories, there are insufficient data to test divergence. Divergence is shown to be plausible in Figs. 16 and 17.

4 Parallelism

Parallelism refers to the property that Regge trajectories of different values of N (which are otherwise identical) are parallel. Two trajectories are parallel if the dynamics are similar. There is no *a priori* reason why parallelism must hold. There are only two ϕ trajectories with $N = 1$ and $N = 2$ which qualify for this test. Fig. 18 shows that the two trajectories appear to be parallel. However these trajectories consist of only 2 or 3 mesons each. It is not clear how they will behave at $J > 2$. The error of $f_2(2010)$ is also quite large compared to the separation of the two trajectories. In conclusion, the status of parallelism as a candidate for a property of Regge trajectories is still uncertain.

5 Conclusion

The linearity of Regge trajectories is clearly violated in Figs. 1, 2, 4 and 6 by simple inspection but is supported by the numerical zone test in Fig. 3. Divergence is not observed on an individual basis. On the other hand, divergence of groups of trajectories of small mass difference is observed on a global level. Due to insufficient data, parallelism is inconclusive.

Currently there are a variety of models predicting both linear and non-linear Regge trajectories. In general, almost all theories [1, 2, 24, 26, 27, 29, 30] agree that meson Regge trajectories are linear in the small J limit. Our plots contradict these predictions. Secondly, all non-linear Regge trajectories models predict trajectories with either increasing or decreasing slopes exclusively, but not both [1, 24, 28]. Our plots show that meson Regge trajectories of both kinds exist. Therefore data rule out all the models that predict non-linear meson Regge trajectories with strictly increasing or decreasing slopes. In the end, data rule out all current meson Regge trajectories models because they are faced with at least one of the problems mentioned above.

6 Acknowledgment

We thank Dr. Sudha Swaminathan and Prof. Dale Snider for their comments. This work was supported in part by NASA Research Grant Numbers NCC-1-354 and NCC-1-260.

References

- [1] E. Di Salvo, L. Kondratyuk and P. Saracco, *hep-ph/9411309*.
- [2] V. V. Andreev and M. N. Sergeenko, *hep-ph/991299*.
- [3] G. F. Chew, *S-Matrix Theory of Strong Interactions*, (W. A. Benjamin, New York, 1961).
- [4] J. J. Sakurai, *Modern Quantum Mechanics*, (Addison-Wesley, Redwood City, California, 1985), 399–410.
- [5] T. Regge, *Nuovo Cim*, **14**, 951 (1959).
- [6] T. Regge, *Nuovo Cim*, **18**, 947 (1960).
- [7] G. F. Chew and S. C. Frautschi, *Phys. Rev. Letters*, **8**, 41 (1962).
- [8] S. C. Frautschi, *Regge Poles and S-Matrix Theory*, (W. A. Benjamin, New York, 1968), 175.
- [9] P. D. B. Collins, *An Introduction to Regge Theory & High Energy Physics*, (Cambridge University Press, Cambridge, 1977).
- [10] R. Ommes and M. Froissart, *Mandelstam Theory and Regge Poles*, (W. A. Benjamin, New York, 1963).
- [11] J. R. Forshaw and D. A. Ross, *Quantum Chromodynamics and the Pomeron*, (Cambridge University Press, Cambridge, 1997), 13–17.
- [12] S. Weinberg, *The Quantum Theory of Fields*, (Cambridge University Press, Cambridge, 1995), 468–469.
- [13] C. B. Chiu, *Annual Review of Nuclear Science*, **22**, 255 (1972).
- [14] E. Segrè, *Nuclei and Particles*, (Benjamin/Cummings, Menlo Park, California, 1982), 832.
- [15] S. Veseli and M. G. Olsson, *hep-ph/9606257*.
- [16] J. M. Cornwall, *Nuclear Physics B*, **128**, 75 (1977).

- [17] J. S. Kang and H. J. Schnitzer, *Physical Review D*, **12**, 841 (1975).
- [18] A. D. Martin and T. D. Spearman, *Elementary Particle Theory*, (Wiley, New York, 1970), 427.
- [19] D. Kahana, K. Maung Maung and J. W. Norbury, *Physical Review D*, **48**, 3408 (1993).
- [20] S. Godfrey and N. Isgur, *Physical Review D*, **32**, 189 (1985).
- [21] W. K. Tang, *Physical Review D*, **48**, 2019 (1993).
- [22] A. Brandt, S. Erhan, A. Kuzucu, D. Lynn, M. Medinnis, N. Ozdes, P. E. Schlein, M. T. Zeyrek and J. G. Zweizig, *Nuclear Physics B*, **514**, 3 (1998).
- [23] L. Burakovsky, *hep-ph/9810296*.
- [24] M. M. Brisudová, L. Burakovsky and T. Goldman, *Physical Review D*, **61**, 054013 (2000).
- [25] D. Haidt and P. M. Zerwas, *The European Physical Journal C*, **3**, 109 (1998).
- [26] H. Grosse and A. Martin, *Particle Physics and the Schrödinger Equation*, (Cambridge University Press, Cambridge, 1997).
- [27] S. Filipponi, *Physical Review D*, **58**, 016003 (1998).
- [28] A. Inopin and G. S. Sharov, *hep-ph/9905499*. (We refer only to the results of the string models for meson trajectories in Fig. 8 of this paper.)
- [29] G. M. Prosperi, *hep-ph/9906237*.
- [30] M. Baldicchi, *hep-ph/9911268*.

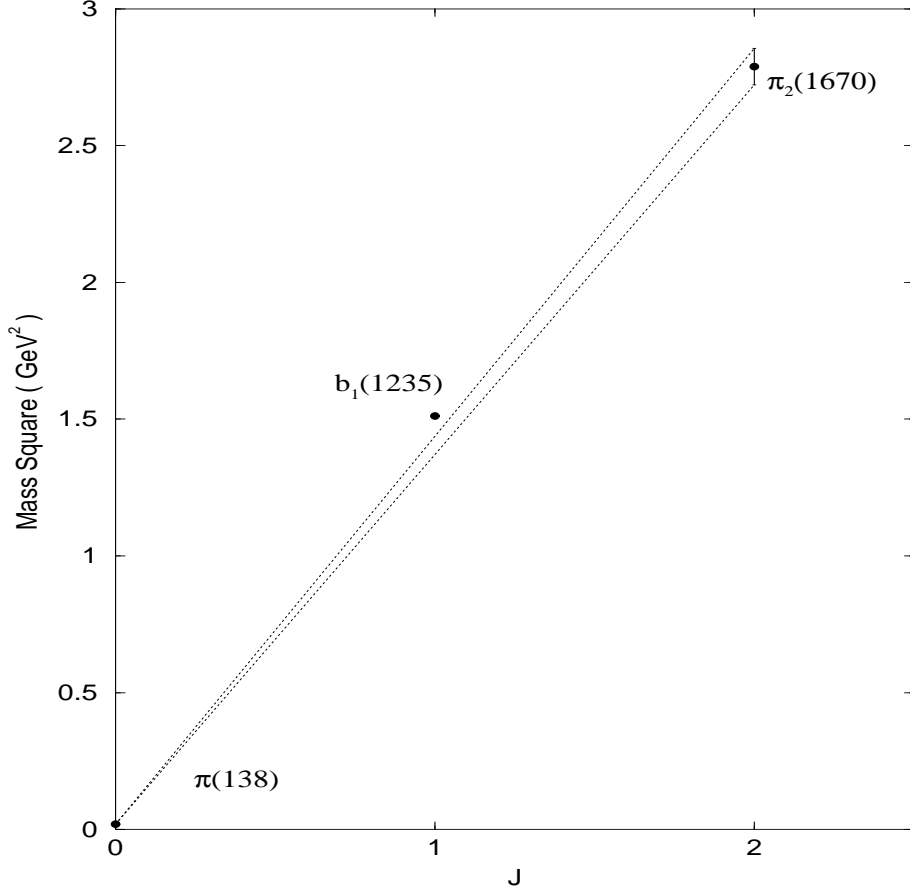


Figure 1: Meson Regge trajectory of the $N = 1$, $S = 0$ singlet states. $b_1(1235)$ fails to intersect the zone. The polynomial fit is $M^2 = -0.1077J^2 + 1.6003J + 0.019$ (GeV²). The mass of $\pi(138)$ is taken to be the average of the masses of $\pi^0(135)$ and $\pi^\pm(140)$. Although there is a 6.5 % difference between the mass squares of $\pi^0(135)$ and $\pi^\pm(140)$, the test zone is virtually unchanged by this small difference because of the large mass squared of the other two mesons on the trajectory. The zone test suggests that the π trajectory is non-linear.

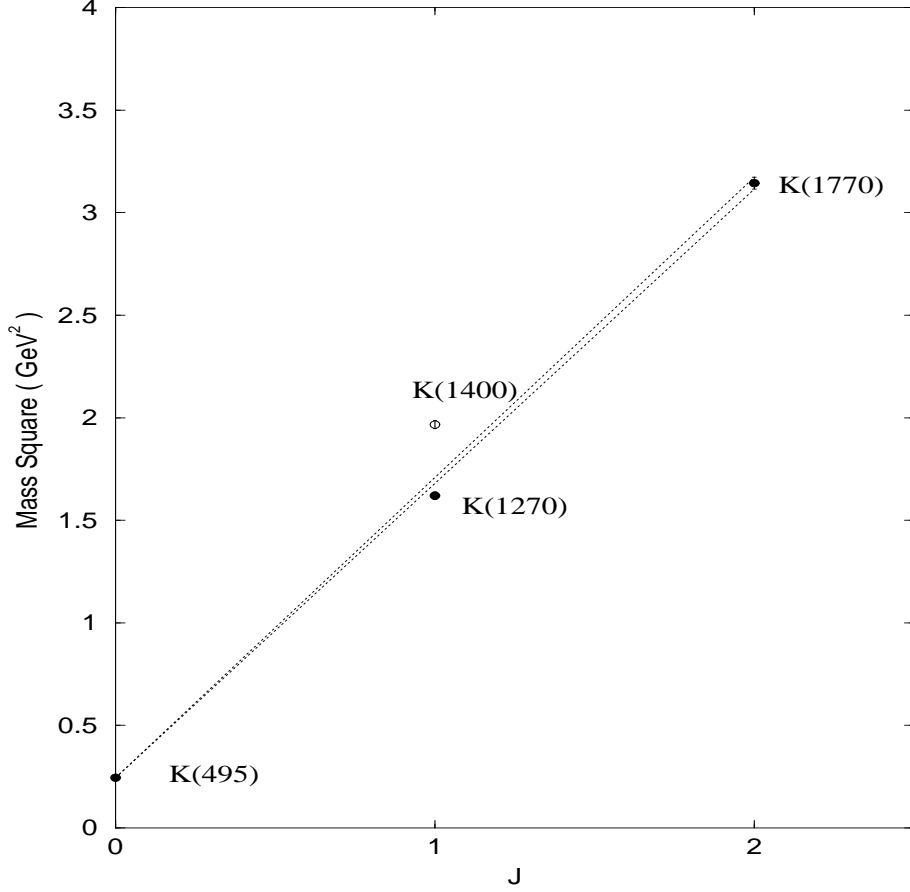


Figure 2: Meson Regge trajectory of the $N = 1$, $S = 0$ singlet states. The RPP assignment table lists K_{1B} as a nearly equal mixture of $K(1270)$ and $K(1400)$. In the graph above, we plot both constituent mesons at $J = 1$ for the sake of completeness. Neither $K(1270)$, $K(1400)$ nor their average satisfies the zone test by simple inspection. The polynomial fit of $K(495)$, $K(1270)$ and $K(1770)$ is $M^2 = 0.0737J^2 + 1.3018J + 0.245 \text{ (GeV}^2\text{)}$.

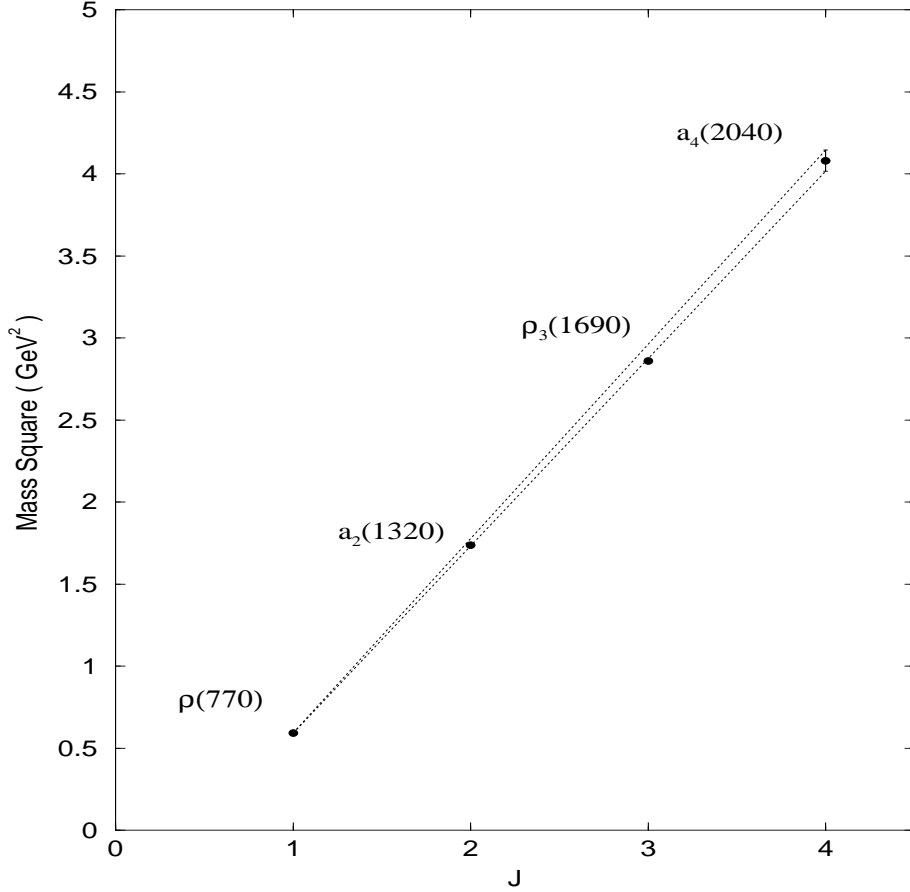


Figure 3: Meson Regge trajectory of the $N = 1$, $S = 1$ third triplet states. Both $a_2(1320)$ and $\rho_3(1690)$ intersect the zone and hence this trajectory passes the zone test. Linearity is supported by the numerical zone test. The polynomial fit is $M^2 = 0.0191J^2 + 1.0629J - 0.4831$ (GeV²). The negative vertical intercept corresponds to a non-sense pole because $J < 1$ is not allowed in an $S = 1$ state.

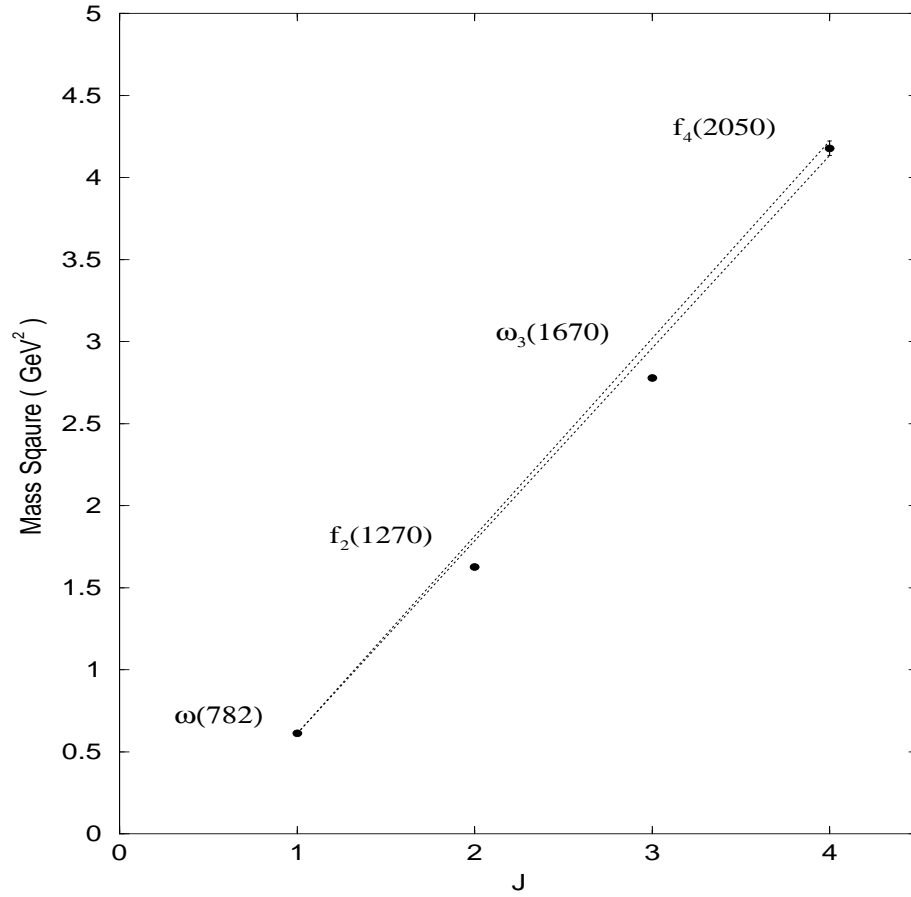


Figure 4: Meson Regge trajectory of the $N = 1$, $S = 1$ third triplet states. Both $f_2(1270)$ and $\omega_3(1670)$ fail to intersect the zone. The polynomial fit is $M^2 = 0.0962J^2 + 0.7042J - 0.1837 \text{ (GeV}^2\text{)}$.

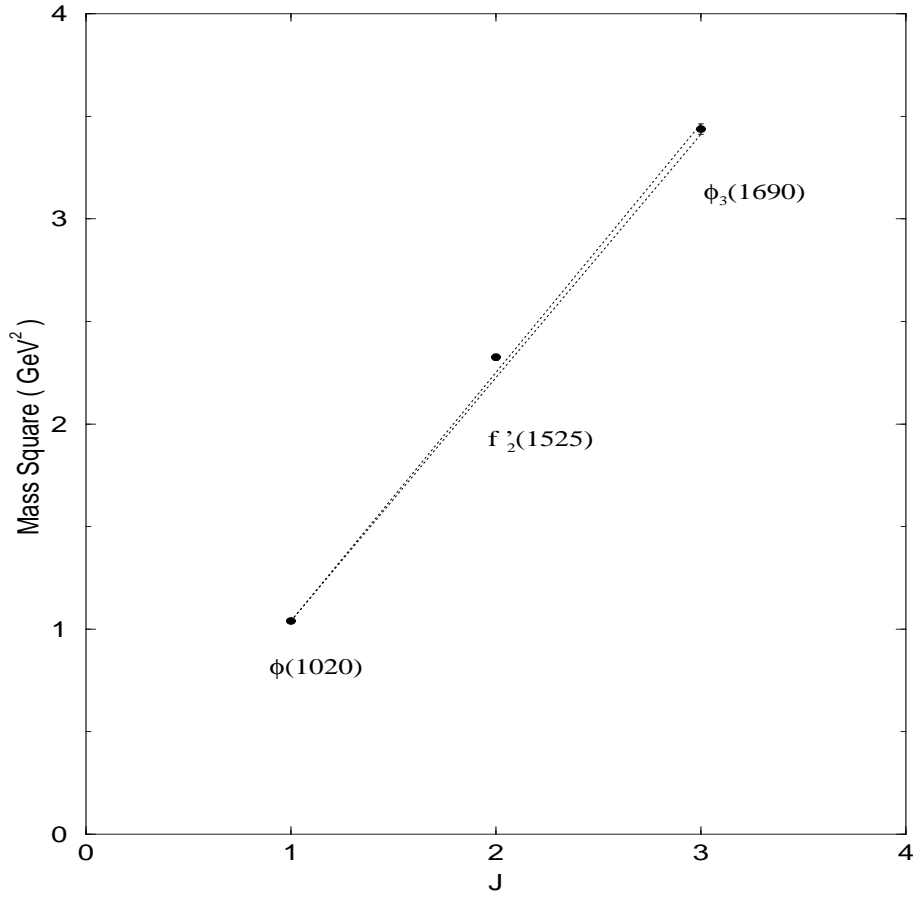


Figure 5: Meson Regge trajectory of the $N = 1$, $S = 1$ third triplet states. $f_2'(1525)$ fails to intersect the zone. The polynomial fit is $M^2 = -0.0879J^2 + 1.5505J - 0.4234 \text{ (GeV}^2\text{)}$.

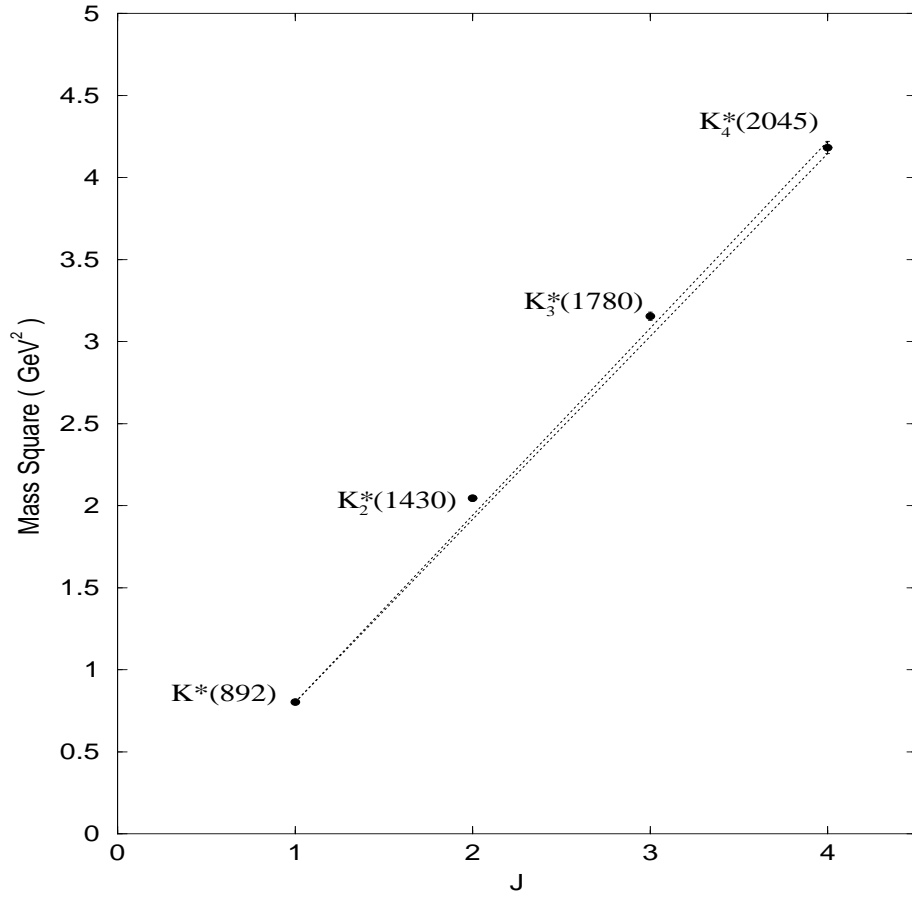


Figure 6: Meson Regge trajectory of the $N = 1$, $S = 1$ third triplet states. Both $K_2^*(1430)$ and $K_3^*(1780)$ fail to intersect the zone. The polynomial fit is $M^2 = -0.0535J^2 + 1.3922J - 0.5331$ (GeV²).

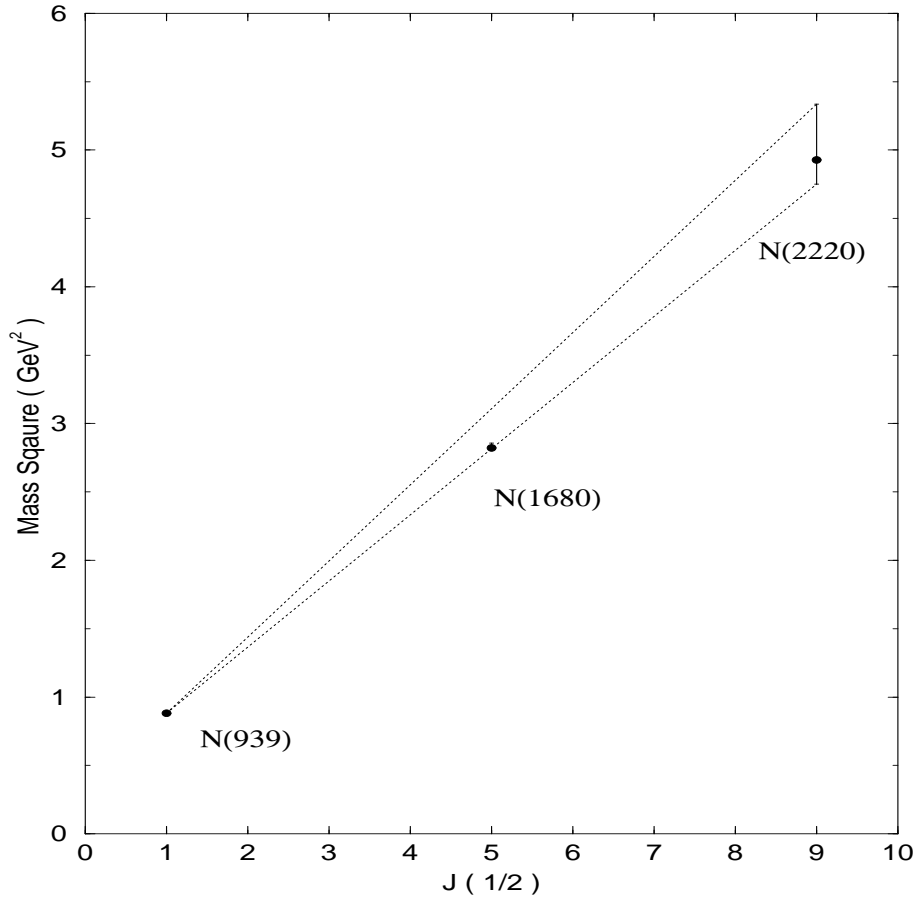


Figure 7: Baryon Regge trajectory of $S = 1/2$, $P = +$ and $I = 1/2$ octet states. $N(1680)$ satisfies the zone test by simple inspection. The polynomial fit is $M^2 = 0.0207J^2 + 0.9081J + 0.4223$ (GeV).

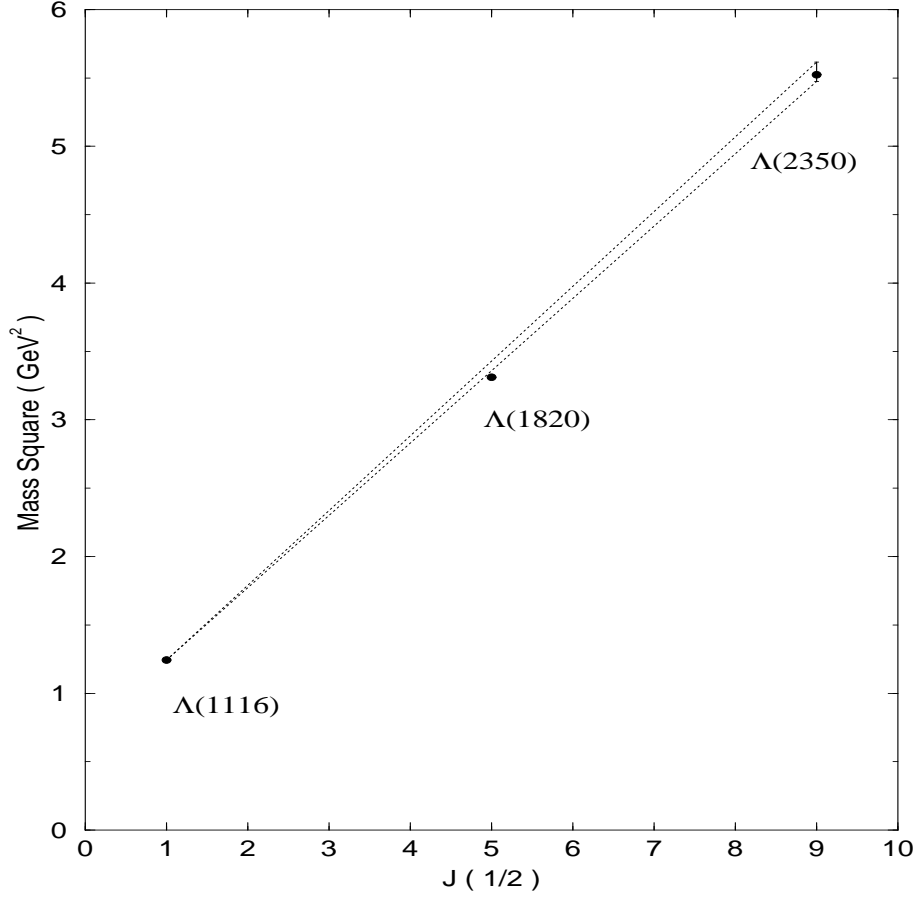


Figure 8: Baryon Regge trajectory of $S = 1/2$, $P = +$ and $I = 0$ octet states. $\Lambda(1820)$ has a numerical bound of $(lb, ub)(3, 2) = (3.360, 3.431) \text{ GeV}^2$ which does not intersect the experimental bound of $(3.294, 3.331) \text{ GeV}^2$. $\Lambda(1820)$ fails the numerical zone test. The polynomial fit is $M^2 = 0.0180J^2 + 0.9797J + 0.7524 \text{ (GeV)}^2$.

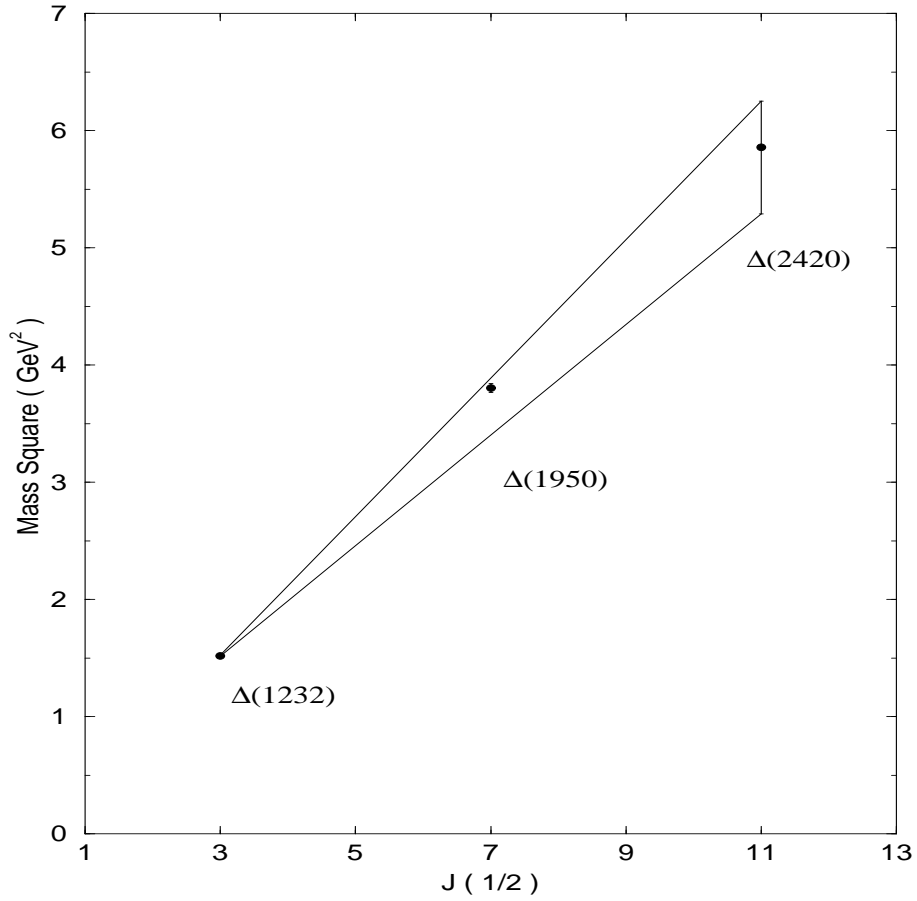


Figure 9: Baryon Regge trajectory of $S = 3/2$, $P = +$ and $I = 3/2$ decuplet states.

$\Delta(1950)$ satisfies the zone test due to the large error of $\Delta(2420)$. The polynomial fit is

$$M^2 = -0.029J^2 + 1.2875J - 0.3480 \text{ (GeV)}.$$

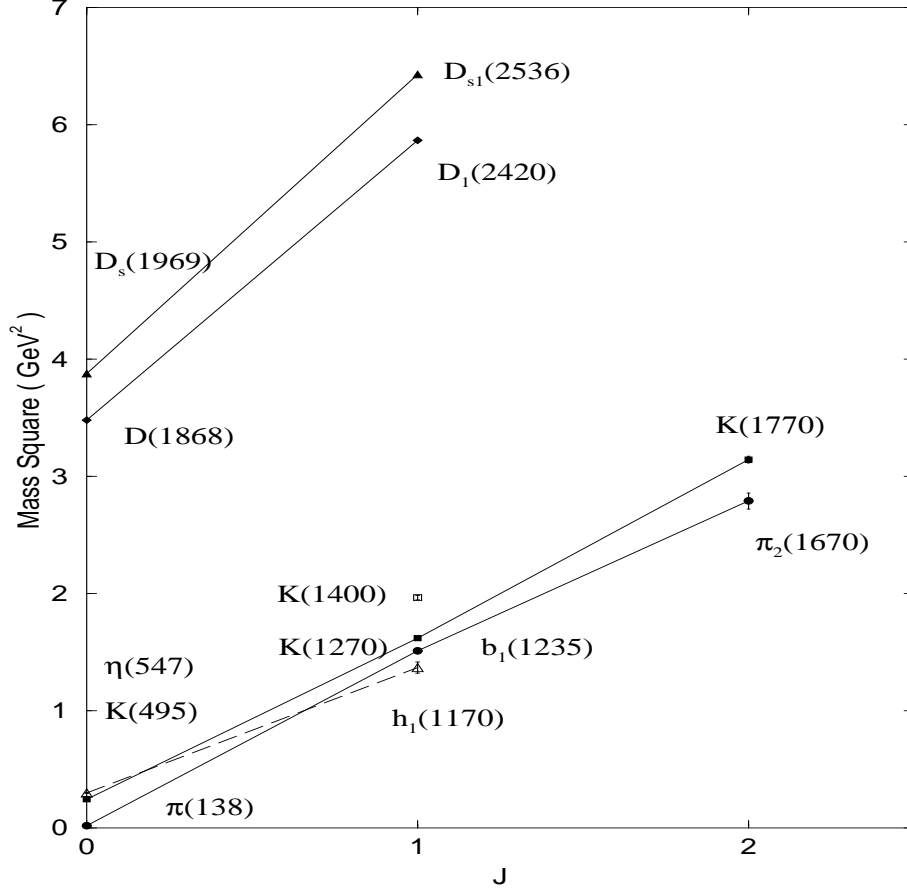


Figure 10: Meson Regge trajectories of the $N = 1$, $S = 0$ singlet states. The series consists of the 1^1S_0 , 1^1P_1 and 1^1D_2 states. The trajectories include those illustrated in Figs. 1 and 2 as well as the D mesons. The D and D_s mesons form a group and the K and light unflavored mesons η and π form another. Global divergence is observed among groups of trajectories of large mass difference but local divergence is violated when the η trajectory (denoted by the dotted line) intersects the K and π trajectories.

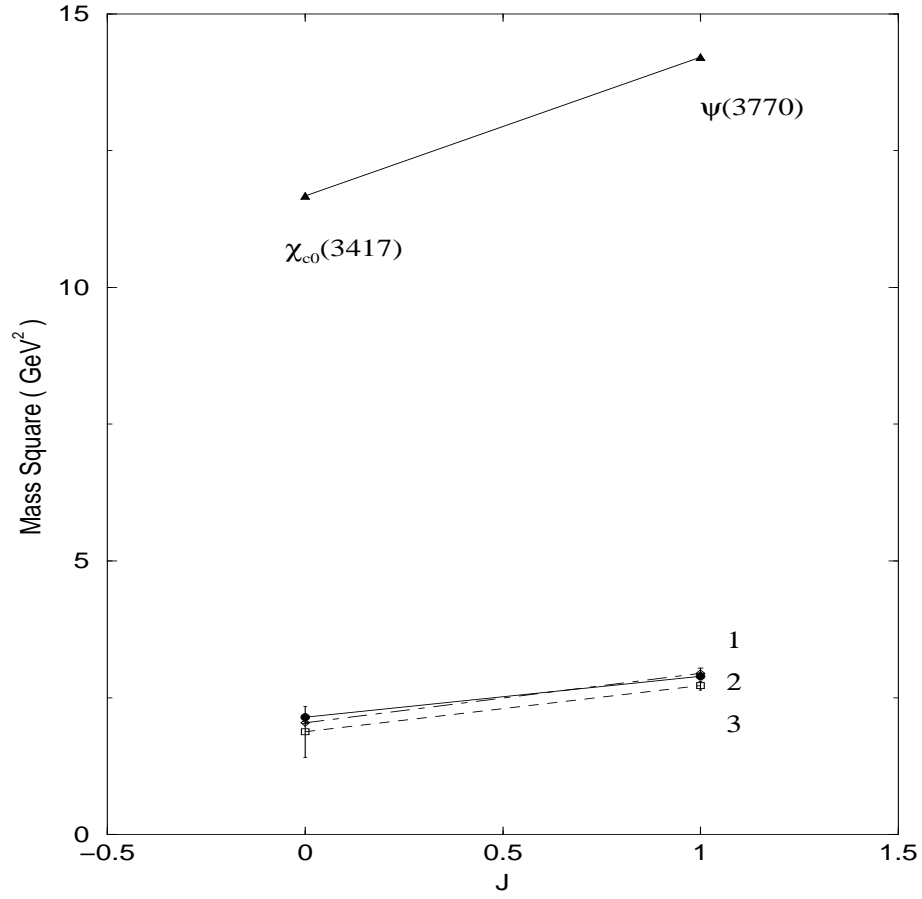


Figure 11: Meson Regge trajectories of the $N = 1$, $S = 1$ first triplet states. The series consists of the 1^3P_0 and 1^3D_1 states. The trajectories labelled 1–3 are magnified in Fig. 12. Global divergence is observed in this graph.

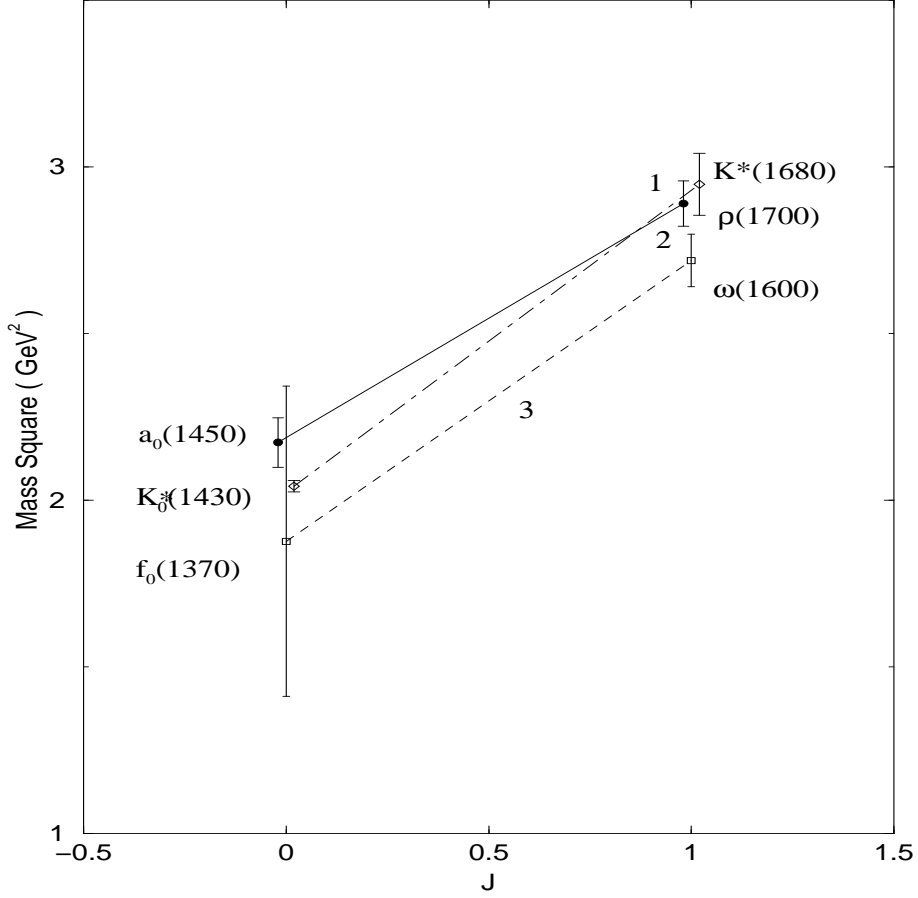


Figure 12: Meson Regge trajectories of the $N = 1$, $S = 1$ first triplet states. The series consists of the 1^3P_0 and 1^3D_1 states. The trajectories 1–3 are the magnifications of a subset of Fig. 11. Trajectories 1 and 2 are shifted horizontally slightly to separate the error bars. Divergence is inconclusive because of the large error bars. The actual mass of $K^*(1680)$ is 1717 MeV which causes it to appear higher than $\rho(1700)$ in the graph.

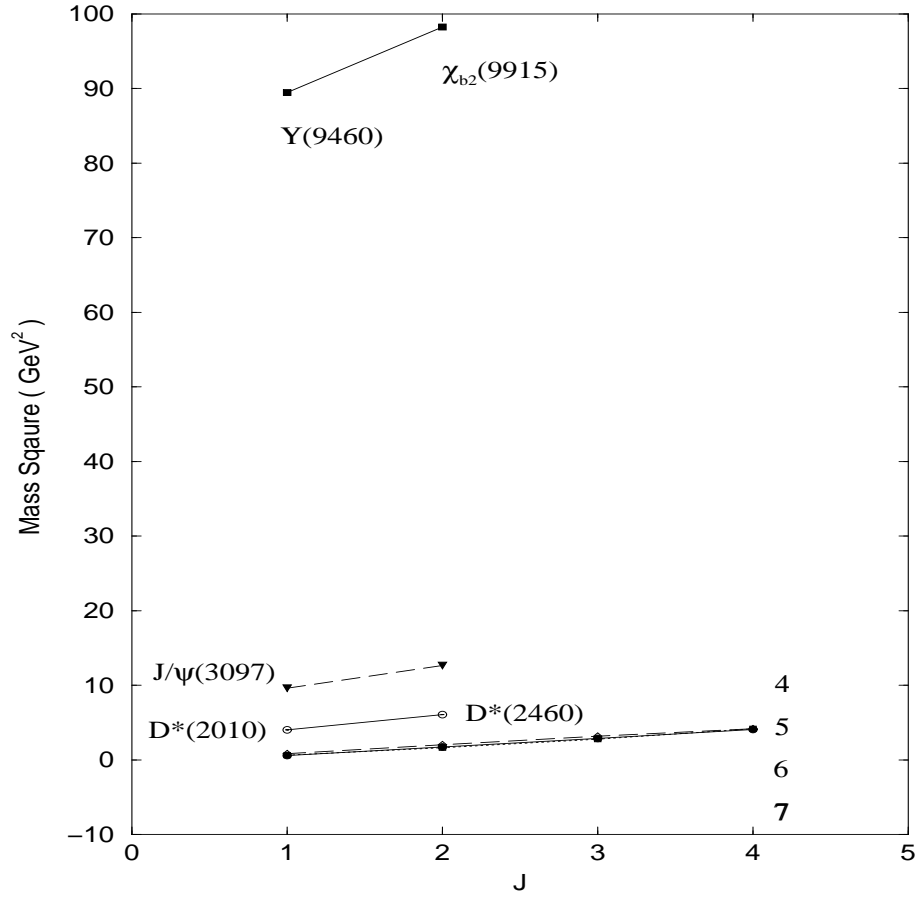


Figure 13: Meson Regge trajectories of the $N = 1$, $S = 1$ third triplet states. The series consists of the 1^3S_1 , 1^3P_2 , 1^3D_3 , and 1^3F_4 states. The group of trajectories labelled 4–7 are magnified in Fig. 14. Global divergence is observed.

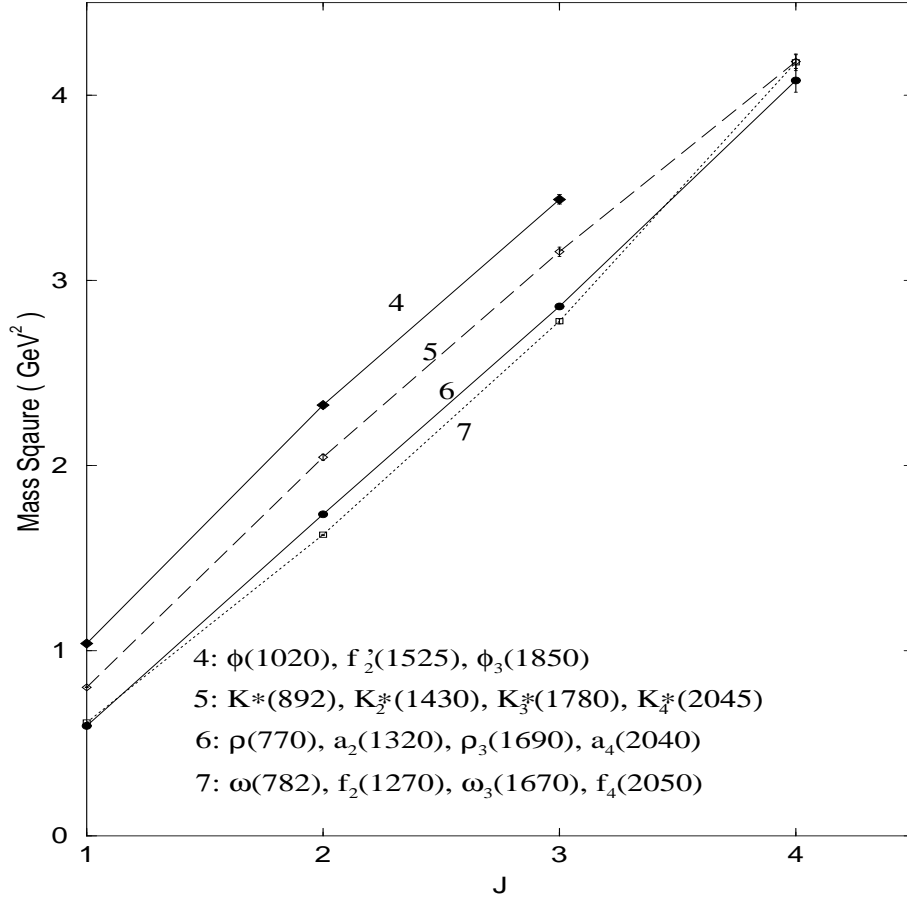


Figure 14: Meson Regge trajectories of the $N = 1$, $S = 1$ third triplet states. The series consists of the 1^3S_1 , 1^3P_2 , 1^3D_3 , and 1^3F_4 states. The trajectories 4–7 are magnifications of a subset of the trajectories in Fig. 13 and are the same trajectories as in Figs. 3–6. Divergence is violated by these trajectories.

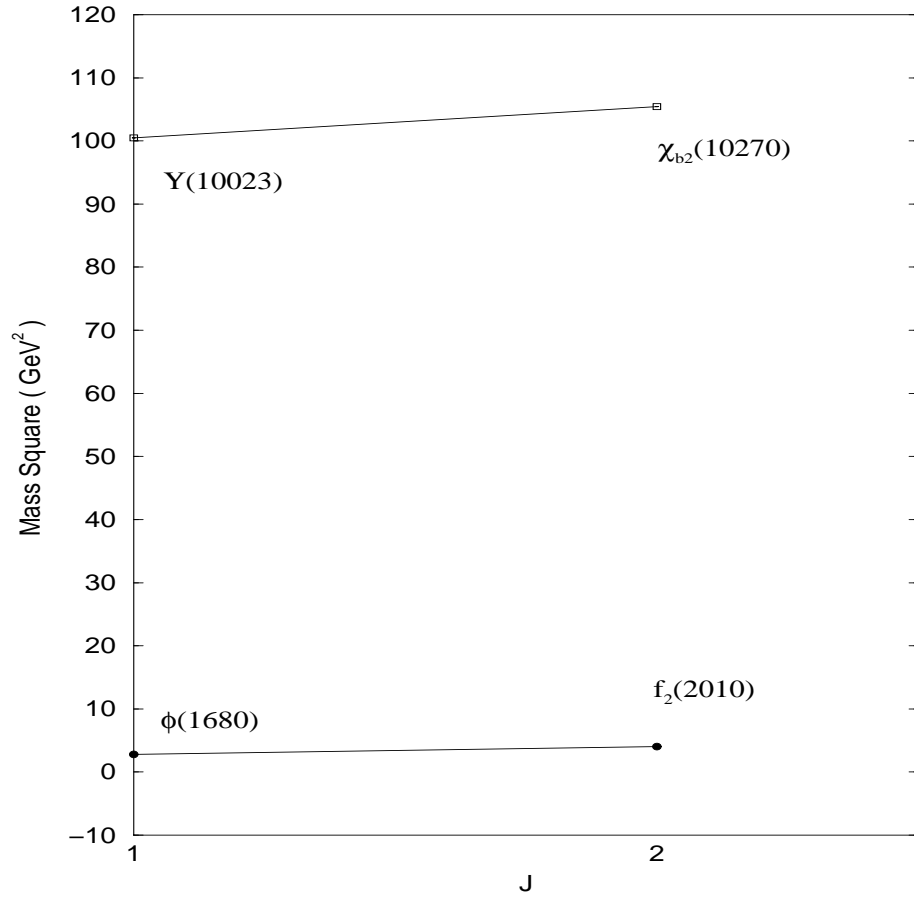


Figure 15: Meson Regge trajectories of the $N = 2$, $S = 1$ third triplet states. The series consists of the 2^3S_1 and 2^3P_2 states. Divergence is observed.

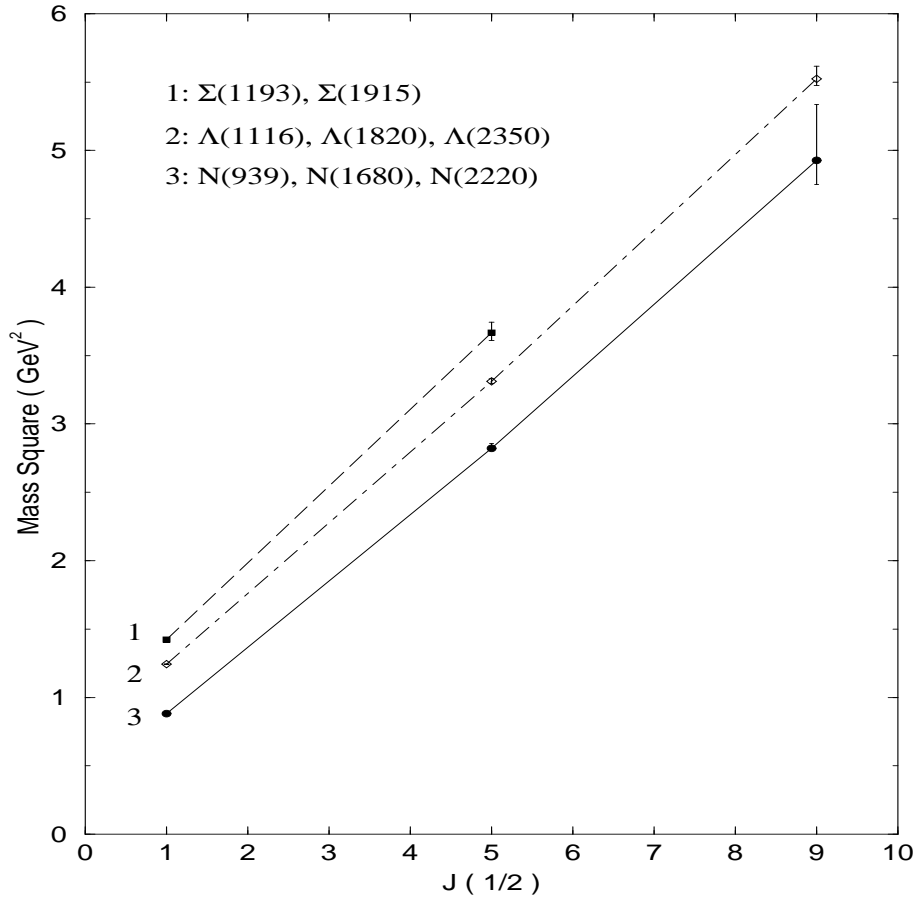


Figure 16: Baryon Regge trajectories of $P = +$ octet states. Due to the scarcity of data and the large error of $N(2220)$, divergence is plausible but inconclusive.

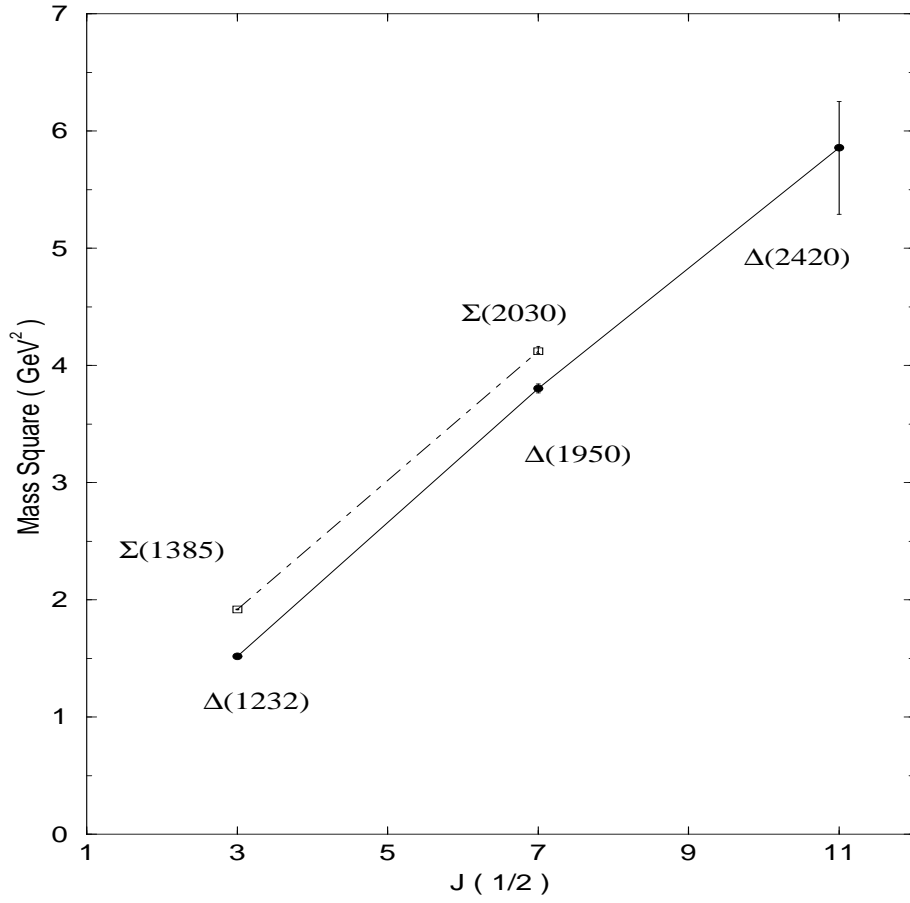


Figure 17: Baryon Regge trajectories of $P = +$ decuplet states. Due to the scarcity of data and the large error of $\Delta(2420)$, divergence is plausible but inconclusive.

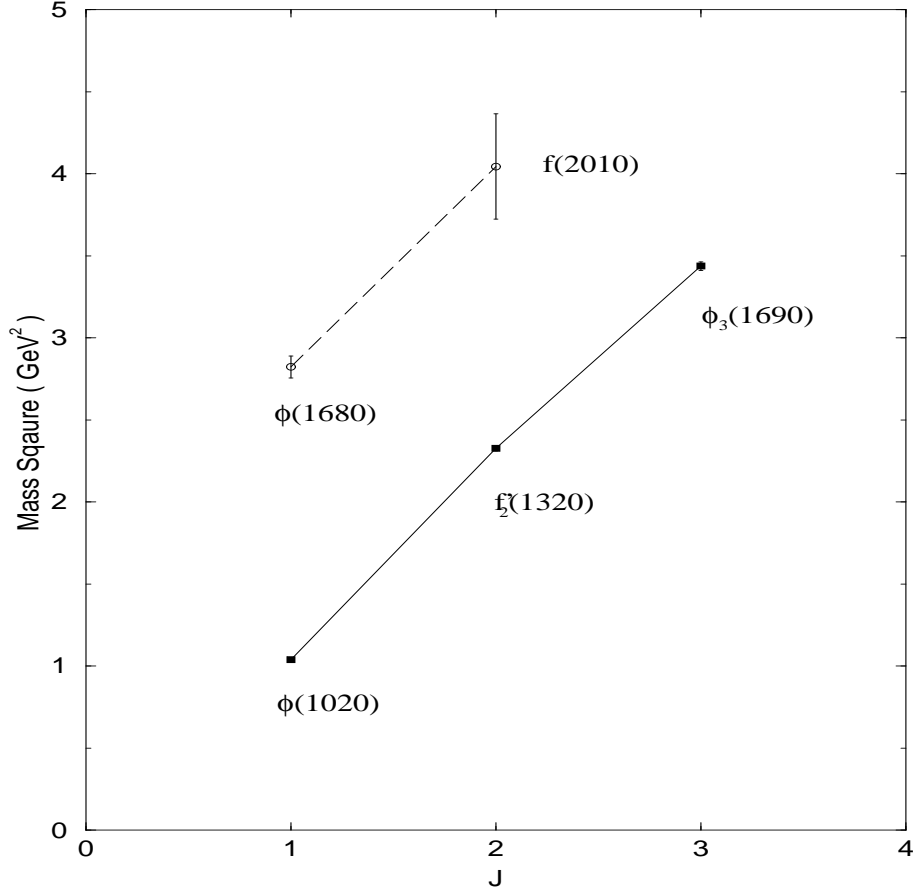


Figure 18: Meson Regge trajectories of the $N = 1, 2$, $S = 1$ third triplet states. The series consists of the 1^3S_1 , 1^3P_2 , 2^3S_1 and 2^3P_2 states. The $N = 1$ states are denoted by solid lines and $N = 2$ states by long-dashed lines. Parallelism is inconclusive due to the large error bar of $f(2010)$.